JACS
JOURNAL OF THE AMERICAN CHEMICAL SOCIETY

ARTICLE

pubs.acs.org/JACS

Surface Supramolecular Organization of a Terbium(III) Double-Decker Complex on Graphite and its Single Molecule Magnet Behavior

Mathieu Gonidec,[†,‡] Roberto Biagi,[§,⊥] Valdis Corradini,[⊥] Fabrizio Moro,[#,§] Valentina De Renzi,[§,⊥] Umberto del Pennino,[§,⊥] Domenico Summa,[∥] Luca Muccioli,[∥] Claudio Zannoni,[∥] David B. Amabilino,[*,†] and Jaume Veciana[*,†,‡]

[†]Institut de Ciència de Materials de Barcelona (ICMAB-CSIC), 08193 Bellaterra, Spain

[‡]Networking Center on Bioengineering, Biomaterials and Nanomedicine (CIBER-BBN), 08193 Bellaterra, Spain

[§]Dipartimento di Fisica, Università di Modena e Reggio Emilia, Modena, Italy

[⊥]S3 Istituto Nanoscienze-CNR, Modena, Italy

[∥]Dipartimento di Chimica Fisica e Inorganica and INSTM, Università di Bologna, Viale Risorgimento 4, IT-40136 Bologna, Italy

Supporting Information Web-Enhanced

ABSTRACT: The two-dimensional self-assembly of a terbium(III) double-decker phthalocyanine on highly oriented pyrolitic graphite (HOPG) was studied by atomic force microscopy (AFM), and it was shown that it forms highly regular rectangular two-dimensional nanocrystals on the surface, that are aligned with the graphite symmetry axes, in which the molecules are organized in a rectangular lattice as shown by scanning tunneling microscopy. Molecular dynamics simulations were run in order to model the behavior of a collection of the double-decker complexes on HOPG. The results were in excellent agreement with the experiment, showing that—after diffusion on the graphite surface—the molecules self-assemble into nanoscopic islands which align preferentially along the three main graphite axes. These low dimension assemblies of independent magnetic centers are only one molecule thick (as shown by AFM) and are therefore very interesting nanoscopic magnetic objects, in which all of the molecules are in interaction with the graphite substrate and might therefore be affected by it. The magnetic properties of these self-assembled bar-shaped islands on HOPG were studied by X-ray magnetic circular dichroism, confirming that the compounds maintain their properties as single-molecule magnets when they are in close interaction with the graphite surface.

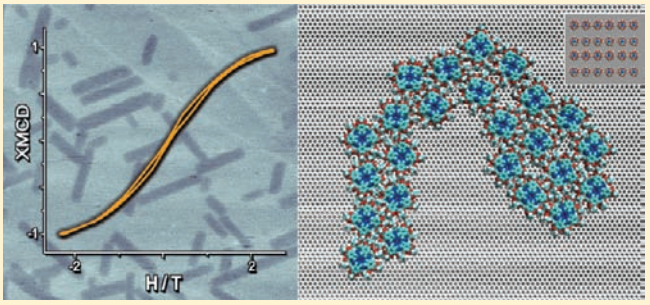

INTRODUCTION

Single-molecule magnets (SMMs) are molecular compounds with a high spin ground state showing a slow magnetization relaxation rate at low temperatures.[1,2] Unlike bulk magnets, these superparamagnetic species do not present a permanent remnant magnetization, but some of them (like the well-known dodecamanganese clusters) have been shown[3] to maintain a remnant magnetization over several months if kept at a sufficiently low temperature below their blocking temperature,[1] at which the relaxation time of the magnetization becomes as fast as the characteristic time of the experiment used to measure it. Since they typically present nanometric dimensions, they are potential candidates for high-density data storage if properly organized on surfaces, with the ultimate goal of storing 1 bit per molecule.[4] Another possible application for such molecules could be in molecular spintronics.[5−7] Nevertheless, some issues need to be addressed for them to be technologically exploitable, like their very low blocking temperature and the difficulties to organize and address individual molecules on surfaces.[8] While a lot of effort has been dedicated over the past few years to the preparation of new SMMs, trying to push-up their blocking temperatures (typically of the order of 5 K for the best compounds), very little has been done toward the addressing of an array of independent magnetic molecules. More importantly, a first step toward any technological application is to check that the properties of SMMs can be preserved when deposited on a surface, and this has been the subject of a very limited number of publications.[9−13]

The double-decker phthalocyanine complexes of some lanthanide ions (Pc_2Ln, in Chart 1), formed by the metal ion sandwiched between two phtalocyanine (Pc) dianionic ligands, have been shown recently to behave either in bulk, in dilute solid solutions, and even in a frozen glass solution as single molecule magnets.[14−17] On the other hand, some functionalized Pc_2Ln complexes were also shown to form well ordered self-assembled domains when deposited on highly oriented pyrolitic graphite (HOPG), although no information about the magnetic properties

Received: October 15, 2010
Published: April 12, 2011

   dx.doi.org/10.1021/ja109296c | J. Am. Chem. Soc. 2011, 133, 6603–6612

Chart 1

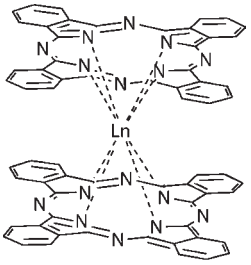

of such two-dimensional (2D) supramolecular organizations was available.[18,19]

As part of an ongoing program on multifunctional double-decker complexes, we have focused on the preparation and characterization of 2D arrays of double-decker phthalocyanine complexes of type Pc_2Ln. Earlier studies showed that complexes bearing peripheral butoxy substituents formed nicely ordered 2D arrays on graphite but that the stability of those assemblies was limited to a few hours because the structured monolayers collapsed overnight.[18] For this reason we chose to prepare long alkoxy chain substituted complexes, in order to increase the number of van der Waals interactions with the substrate, so as to stabilize the monolayers. The known acetal protected complex $^{i}Pc_2Tb$ (**1**)[20] was envisaged initially as a protected reaction intermediate toward a variety of alkoxy terminated phthalocyanines, and accordingly it was prepared. However, during the course of this ongoing research program it was observed serendipitously that $^{i}Pc_2Tb$ complex self-assembles as 2D crystals on HOPG.

Here we present a detailed experimental and theoretical study of such 2D supramolecular organizations on graphite as well as the magnetic behavior of such organizations characterized by X-ray magnetic circular dichroism (XMCD) comparing them with the bulk magnetic properties of this SMM.

EXPERIMENTAL SECTION

The starting materials were purchased from Sigma-Aldrich and used without any further purification. ^{1}H NMR spectra were recorded on a Bruker Avance DPX-360 spectrometer. The nondeuterated solvent peak was used as an internal reference to calibrate the spectra ($CDCl_3$, 7.26 ppm). Mass spectra were recorded on a Bruker Ultraflex LDI-TOF spectrometer. UV−vis absorption spectra were collected on a Varian Cary 5000 spectrometer.

Synthesis and Characterization. *4,5-Dibromocatechol (**2**).* In a 500 mL three-neck round-bottom flask under nitrogen, equipped with a reflux condenser, an addition funnel and a gas outlet connected to a bubbler filled with a 10% NaOH aqueous solution was suspended catechol (136 mmol, 15.0 g, 1 equiv) in CCl_4 (150 mL). Bromine (272 mmol, 43.5 g, 2 equiv) diluted in CCl_4 (20 mL) was added dropwise at 0 °C over 4.5 h. The excess of bromine was neutralized with aqueous $NaHSO_3$ (150 mL, 40% solution). The mixture was filtered, and the solids were dissolved in CCl_4, washed with water, and dried in vacuum. The obtained 4,5-dibromocatechol (30.2 g) was then recrystallized from $CHCl_3$ (220 mL) to afford a white crystalline solid (22.5 g, 84.0 mmol) with a yield of 62%. ^{1}H NMR (250 MHz, $CDCl_3$): δ 7.14 (s, 2 H, Ar−H), 5.43 (s, 2 H, −OH) ppm.

*5,6-Dibromo-2,2-dimethyl-1,3-benzodioxole (**3**).* Phosphorus trichloride (7.5 mmol, 0.65 mL, 0.4 equiv) was added dropwise at 20 °C over 30 min to a suspension of 4,5-dibromocatechol (18.7 mmol, 5.0 g, 1.0 equiv) and acetone (1.644 mL, 22.4 mmol, 1.2 equiv) in dry toluene (30 mL). The reaction was stirred overnight at room temperature. Potassium carbonate (25 g) was added, and the solids were filtered and washed with toluene (50 mL). The organic layer was then washed with 10% NaOH (4 × 50 mL) dried on $MgSO_4$, and the volatiles were evaporated on a rotatory evaporator affording 5,6-dibromo-2,2-dimethyl-1,3-benzodioxole (2.4 g, 42%). FT-IR: 3110 (w), 3058 (w), 2991 (w), 2929 (w), 1697 (w), 1649 (w), 1600 (w), 1488 (s), 1459 (m), 1379 (s), 1362 (m), 1259 (m), 1239 (s), 1206 (m), 1078 (m), 980 (m), 914 (m), 855 (s), 827 (w), 782 (m), 693 (w), 659 (w), 595 (w), 516 (m) cm^{-1}. ^{1}H NMR (250 MHz, $(CD_3)_2CO$): δ 7.12 (s, 2H, Ar−H), 1.69 (s, 6H, $-C(CH_3)_2$) ppm.

*4,5-Isopropylidenedioxyphthalonitrile (**4**).* In a dry round-bottom flask under argon, 5,6-dibromo-2,2-dimethyl-1,3-benzodioxole (9.99 mmol, 3.08 g, 1.0 equiv), tetrakis(triphenylphosphine) palladium(0) (0.99 mmol, 1.15 g, 0.1 equiv), and zinc cyanide (12.0 mmol, 1.41 g, 1.2 equiv) in DMF (20 mL) were suspended. The mixture was then heated at 120 °C for 2 h after which ammonia (37%, 100 mL) was added, and the resulting precipitate was filtered, washed with more ammonia (100 mL), and purified by column chromatography on silica gel using toluene as an eluent, affording 4,5-isopropylidenedioxyphthalonitrile (1.7 g, 85%) as a white solid. FT-IR: 3123 (w), 3067 (w), 2995 (w), 2943 (w), 2229 (s), 1741 (w), 1651 (w), 1598 (m), 1546 (w), 1501 (s), 1452 (m), 1402 (w), 1381 (s), 1282 (s), 1264 (m), 1255 (m), 1210 (s), 1165 (m), 1119 (m), 982 (s), 879 (s), 873 (s), 826 (s), 775 (m), 731 (w), 654 (m), 534 (s), 513 (w) cm^{-1}. ^{1}H NMR (250 MHz, $CDCl_3$): δ 7.05 (s, 2H, Ar−H), 1.75 (s, 6H, $-C(CH_3)_2$) ppm.

*Bis-(tetrakis-isopropylidenedioxy-phthalocyaninato) terbium(III) ($^{i}Pc_2Tb$; **1**).* In a flame-dried Schlenk tube under argon, 4,5-isopropylidenedioxyphthalonitrile (0.5 mmol, 100 mg, 1.0 equiv) was introduced, and then the tube was degassed and purged with argon three times. Dry hexanol (1.5 mL) was added with a syringe. DBU (0.25 mmol, 38 mg, 0.5 equiv) was added, and after stirring for 5 min under argon, $Tb(OAc)_3 \cdot [H_2O]_6$ (0.08 mmol, 35 mg, 0.16 equiv) was added at once. The mixture was then warmed up in a sand bath to reflux at 160 °C for 16 h. The course of the reaction was monitored by UV−vis. After this time, the mixture was cooled to room temperature, and acetonitrile was added to precipitate the complex. The dark-green precipitate was filtered and dried in air. It was then purified by column chromatography with silicagel and, by repeated size exclusion chromatography (on Biobeads SX1) used in both cases, toluene as an eluent. The title compound was obtained (21 mg, 19%) as a dark-green powder. MS m/z: 1759 (M^+). FT-IR: 2985 (w), 2921 (w), 2852 (w), 2782 (w), 1732 (w), 1599 (w), 1456 (s), 1387 (s), 1315 (m), 1270 (s), 1206 (s), 1125 (m), 1068 (s), 1010 (m), 976 (s), 860 (s), 837 (s), 752 (m), 723 (m), 680 (w) cm^{-1}. UV−vis (log(ε), toluene): 292 (4.90), 336 (4.90), 371 (5.03), 483 (4.52), 581 (4.17), 605 (4.40), 667 (5.13) nm.

Atomic force microscopy. The atomic force microscopy (AFM) images were recorded on a PicoSPM system (Molecular Imaging). The intermittent contact mode was used close to resonance frequencies of the silicon cantilevers (Nanosensors, FM type force constant 1.2−3.5 N/m and tip diameter 5 nm) of around 60−70 kHz. All the images were recorded under atmospheric conditions.

Scanning tunneling microscopy. The scanning tunneling microscopy (STM) images were recorded in ultrahigh vacuum on a VT-SPM system (Omicron). Imaging conditions were a tunneling current of 50 pA and a bias voltage of −0.4 V.

Magnetometry. The magnetization measurements of bulk samples were done on a Quantum Design PPMS magnetometer equipped with a Vibrating Sample Magnetometer (VSM). The sample consisted of 9.17 mg of complex **1** introduced in a gelatin capsule.

Molecular Dynamics (MD) Simulations. We notice first that the complex is expected to assemble spontaneously and to be kept together by the strong electrostatic interactions between the oppositely charged metal and ligands, while its geometry should be determined by a balance between electrostatic interactions and steric repulsions, in

comparison with lanthanide-water complexes.[21] We have thus modeled the structure considering the compounds as (quasi) ionic, without imposing a twist angle but allowing the angle reported (varying from 30° to 45°) to be the result of steric repulsion, polarizability (Lennard-Jones terms) and electrostatic interactions. This is an acceptable approximation for terbium and lanthanides in general (unlike other metals, such as copper) as the character of the bonding within the complexes is strongly ionic.[22,23] In practice we have modeled the neutral $^{i}Pc_2Tb$ complex with an atomistic force field (FF) considering three separate units, a Tb^{4+} cation and two $^{i}Pc^{2-}$ anions, without explicit chemical bonds between them. The general amber force field (GAFF)[24] was used, after specific parametrization for charges and geometrical parameters were obtained, as described below. The optimized geometry and the atomic charges on $^{i}Pc^{2-}$ atoms have been calculated with standard quantum chemistry methods.[25] In practice density functional theory (DFT), with the B3LYP functional and a 6-31G* basis set were employed,[25] using the Gaussian09 software package.[26] The parameters defining the torsional potentials involving aromatic nitrogens in phthalocyaninates were also calculated at this level of DFT theory for a negatively charged fragment of the ^{i}Pc (see Supporting Information for details). The need for this reparameterization stems from the fact that the charged Pc is more rigid than the neutral one, due to its quinoidal character, and its torsional parameters are thus different from those of the general purpose GAFF set, derived for neutral molecules. In the absence of literature data for terbium ions, the Lennard-Jones parameters for Tb^{4+} were arbitrarily set equal to the ones derived for Eu^{3+}/Gd^{3+} by van Veggel et al.[27] ($\sigma = 3.3$ Å, $\varepsilon = 0.05$ kcal/mol). To verify the realism of this choice, we compared the energy-minimized geometry of the complex obtained by our force field with the crystal structure of a similar Tb−phthalocyanines complex present in the Cambridge Crystallographic Database (JERGAP),[28] finding that the distances between Tb^{4+} and the $^{i}Pc^{2-}$ nitrogens were reproduced to within 0.1 Å by the FF, being close to 2.43−2.44 Å in both cases. All the other parameters for the $^{i}Pc_2Tb$ complex were taken from the GAFF force field.[24] We also tested the capability of the force field of reproducing the self-assembling of the three ions constituting the complex through a molecular dynamics (MD) simulation of 20 ps, dealing with separate 6 $^{i}Pc^{2-}$ and 3 Tb^{4+} ions placed on a 36 × 20 × 2 HOPG surface (see movie 1). In this case the results also were satisfactory as complexes easily and quickly came together and self-assembled.

Rectangular, defect-free graphite sheets with a thickness of four atomic layers were built by replicating the crystalline cell of HOPG graphite[29] of 72 × 35 × 2 times (hence four carbon sheets in the z direction). The interaction of graphite atoms with the complexes was parametrized with the well-known Steele's potential,[30,31] using a cutoff of 18 Å. The electrostatic interactions, which act only between the complexes (our model graphite atoms do not bear atomic charges), were calculated with the smooth particle mesh Ewald method, with a mesh size of 1.2 Å. Different ways of modeling thermal exchange between the graphite surface and the complexes were tried, as described in Supporting Information, Section 4. The simple approach of keeping graphite atoms fixed produced aggregates similar in structure to the ones obtained with more elaborate schemes involving surface atom vibrations and will be adopted in what follows, except when stated otherwise.

All MD simulations were run at constant volume and temperature (300 K) using the NAMD code[32] with 3D periodic boundary conditions; the graphite rectangle sides were oriented parallel to the x and y Cartesian axes, and the z box side was set to 600 Å to mimic, in practice, a slab geometry with 2D periodic boundary conditions. A time step of 1 fs was employed for integrating the equations of motion, and simulations of aggregation were typically carried out of for 10 ns.

XMCD Measurements. The XMCD experiments were carried out at the ID8 beamline of the European Synchrotron Radiation Facility (ESRF) in Grenoble (France). The X-ray absorption spectra (XAS) were taken at the $M_{4,5}$ absorption edge of Tb in total electron yield mode using circularly polarized light with about 100% polarization degree. Temperature and external magnetic field were 7 K and up to 5 T, respectively. The measurements were done using an attenuated beam flux in order to avoid radiation exposure induced sample degradation. Integrity checks based on XAS spectra were performed throughout the experiment, never finding any trace of degradation. The direction of the impinging beam was parallel to the applied magnetic field (H), and both were perpendicular to the sample surface. The dichroic spectrum was obtained as the difference between the absorption spectra taken with the helicity of the incident photon antiparallel ($I^{\uparrow\downarrow}$) and parallel ($I^{\uparrow\uparrow}$) to the applied magnetic field (H). This spectrum is then normalized to the maximum intensity of the unpolarized spectrum $1/2(I^{\uparrow\downarrow} + I^{\uparrow\uparrow})$. In the hypothesis that the XMCD spectrum holds its shape, its intensity is proportional to the projection of the magnetic moment of the absorbing atom on the direction of the photon wave vector,[33] therefore the hysteresis curves can be obtained by recording the XMCD signal as a function of the applied magnetic field.

Scheme 1. Synthesis of $^{i}Pc_2Tb$ (1) in Three Steps From 4,5-Dibromocatechol (2) Using a One-Step Methodology from the Corresponding Phthalonitrile 4

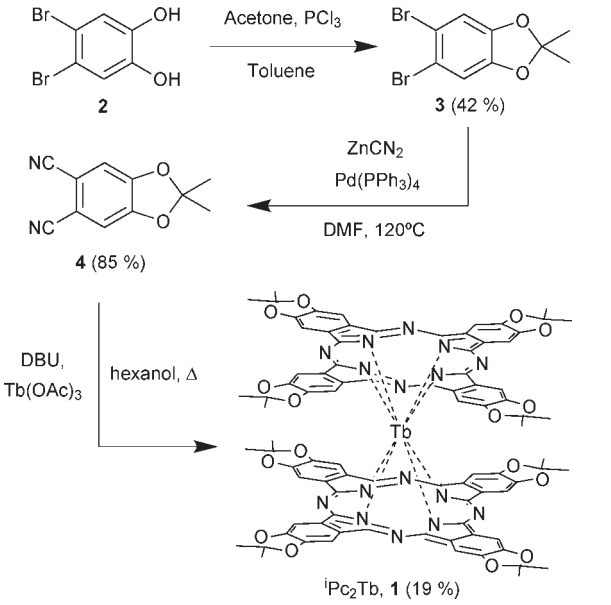

RESULTS AND DISCUSSION

Synthesis. The isopropylidene dioxy-substituted double-decker terbium complex **1** ($^{i}Pc_2Tb$) was prepared in three steps (see Scheme 1) from 4,5-dibromocatechol (**2**) with small changes from an established method.[20]

Compound **3** was prepared from a solution of **2** in toluene with a stoichiometric amount of acetone by the dropwise addition of a solution of PCl_3 in toluene. The corresponding phthalonitrile **4** was prepared in high yield by a tandem zinc−palladium catalyzed cyanation of **3**, instead of employing the classical Rosenmund−von Braun conditions. Indeed, the tandem zinc−palladium method allows the formation of phthalonitriles from 1,2-dibromoaryl derivatives at 120 °C only and with almost stoichiometric amount of zinc cyanide.[34]

These more gentle conditions, as compared to the Rosenmund−von Braun reaction which requires temperatures of around 150 °C and great excess of cyanide, allow preparation

dx.doi.org/10.1021/ja109296c | J. Am. Chem. Soc. 2011, 133, 6603–6612

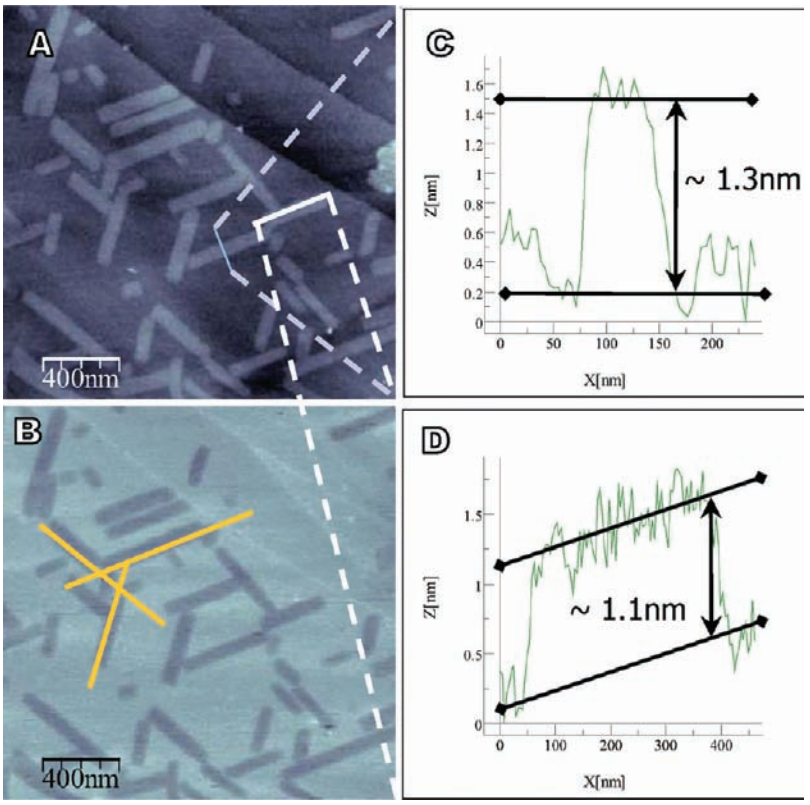

Figure 1. (A) Topography and (B) phase AFM images of the self-assembled bar-shaped islands formed by complex **1** on HOPG as dropcast from a 10^{-6} M solution in toluene. (B) In yellow are depicted the three different orientations of the bars. (C and D) Two profiles showing the thickness of the bars in part (A) are reported.

of the target phthalonitriles in higher yield, avoiding for instance the formation of copper phthalocyanine as an undesired byproduct. Finally, the double-decker terbium complex **1** was achieved by reacting compound **4** with terbium(III) acetate in the presence of DBU in refluxing *n*-hexanol. Complex **1** was obtained as a dark-green powder which is stable at ambient conditions.

Surface Deposition. In order to investigate the self-assembly properties of complex **1**, dilute solutions of the double-decker terbium complex in toluene were prepared. These solutions were dropcast onto freshly cleaved HOPG under ambient conditions. The solvent was allowed to evaporate, and the obtained monolayers were studied, directly after deposition, by atomic force microscopy (AFM) in acoustic mode. The optimal deposition condition corresponded to a 10^{-6} M solution of **1**. Thus, after warming up such a solution with a heat gun, it was dropcast onto freshly cleaved HOPG and covered with a Petri dish in order to obtain a slow and regular evaporation of the solvent, therefore to approach the supersaturation slowly. In these conditions, compound **1** formed highly regular anisotropic bar-shaped islands of a few hundreds of nanometers long by approximately 50 nanometers wide (see Figure 1). It is also worth stressing that these bar-shaped islands are not randomly distributed on the graphite surface. Indeed they are disposed in such a way that they form angles of about 120° among themselves, which is a strong indication that the growth of these supramolecular organizations happens along one of the three main graphite symmetry directions. The anisotropy of these bars can be explained by a difference in the kinetics of crystallization along and across the graphite main axes. Namely, the crystallization rate is higher along one of the substrate's axes, while the lateral growth seems to be less favored. The height or thickness of the self-assembled nanoislands was of approximately 1.1−1.3 nm, as shown in Figure 1C and D. The tops of the bar-shaped islands are relatively smooth, indicating a high degree of structural order, as is expected in a crystalline material.

Ideally, the expected height of a monolayer of molecules of complex $^{t}Pc_2Tb$, when arranged flat on graphite, can be estimated by summing the interplanar distance of the two phthalocyanine rings, plus two times the distance of the outer hydrogen atoms from the plane of the phthalocyanine ligands, and two times the van der Waals radius of hydrogen (see Figure 2). The interplanar distance of the complex was estimated to be of 3.9−4.0 Å from the X-ray structure of another neutral double-decker phthalocyanine complex.[35] The distance of the outer hydrogen atom from the plane of the phthalocyanines was estimated to be of approximately 2.0 Å from the crystal structures of other benzodioxole compounds[36] and confirmed by PM3 molecular mechanics on 2,2-dimethyl-benzo dioxolane. Finally, a value of 1.1 Å was used as the van der Waals radius of hydrogen.[37] The total estimated height of the monolayers on graphite is then 10.1−10.2 Å, i.e., 1.0 nm. On the other hand, the diameter of the complex was estimated to be of approximately 22.8 Å or 2.3 nm, i.e., 20.6 Å plus two times the van der Waals radius of hydrogen. Therefore, all of these estimated dimensions suggest strongly that the double-decker molecules should lay flat on the surface, and the bar-shaped nanoislands are one-molecule thick. These estimated dimensions are in very good agreement with the MD simulations.

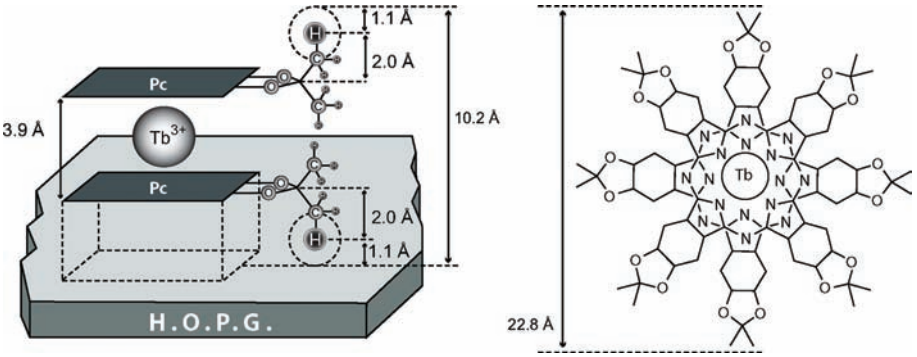

Figure 2. Schematic representation of complex $^{i}Pc_{2}Tb$ on top of the graphite (left) and the lateral dimensions of the complex (right).

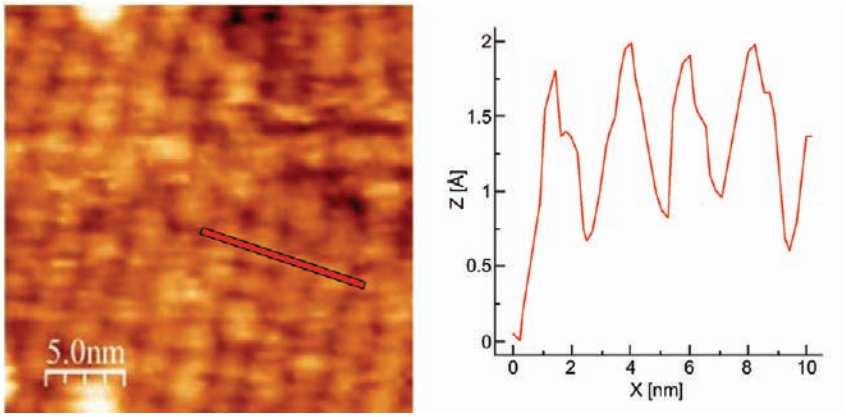

Figure 3. (left) STM image of the self-assembled layer formed by complex **1** on HOPG as dropcast from a 10^{-6} M solution in toluene. (right) Depth profile measured across four rows of molecules. The distance from one row to the other is approximately 2.1−2.3 nm.

The morphology of bar-shaped nanoislands could be seen over large areas of the sample, in different locations of the graphite, and on different samples. The size distribution of the nanoislands on the graphite was estimated by measuring 170 different bar-shaped islands. The width of the nanocrystals was thus estimated to be of $w = 70 \pm 30$ nm, and their length $l = 250 \pm 150$ nm indicating that they correspond to 2D crystals of approximately $1 \times (30 \pm 13) \times (108 \pm 65)$ molecules. This value agrees with that of ∼5000 molecules calculated from the simulation using the surface area per molecule obtained for the supramolecular aggregates by MD (vide infra).

In order to get more insight into the internal organization of the nanoislands, a dropcast sample prepared from a 10^{-6} M solution of **1** in toluene—employing the same deposition conditions as those used for the AFM experiment—was studied by STM. Complex **1** was shown to form packed layers composed of ordered rows of molecules (see Figure 3).

The structure of the layer was found to be rectangular. Interestingly, the distance between adjacent rows of molecules was found to be of approximately 2.1−2.3 nm which is in good agreement with the estimated lateral dimensions of complex **1** (see Figure 2).

Molecular Dynamics Simulations. In order to confirm and enrich the experimental observations, various room temperature MD studies were performed, changing the number of complexes (9, 16, 24) and the dimensions of the graphite surface ($36 \times 20 \times 2$, $60 \times 40 \times 2$, $72 \times 35 \times 2$), while always keeping low coverage, submonolayer conditions. In the following, we report the results of the large samples only, but in all of these simulations, as described below, the $^{i}Pc_{2}Tb$ complexes exhibited the tendency to lay flat ("face-on") on the surface and not to stack one onto each other to form π-aggregates. In each complex we observed that the two phthalocyaninates groups are twisted with respect to each other, with an angle varying from 30° to 45° (cf. also movies 1−2), a conformation similar to that of other terbium(III) double-decker phtalocyanine complexes.[12] This is probably due to the need to minimize, on one hand, the steric repulsion between the methyl groups and, on the other hand, the electrostatic repulsion between equivalent (thus bearing the same atomic charge) atoms on the two moieties. We also notice that this conformation allows some interaction between the arms of the uppermost $^{i}Pc^{2-}$ and the substrate. Isolated and aggregated complexes show also a preferential orientation of the $^{i}Pc^{2-}$ arms with respect to one of three equivalent graphite axes; typically, one of the two arms of the lowermost $^{i}Pc^{2-}$ is on average parallel to one of the axes, with angular displacements of about 10° (see Figure 4). As a matter of fact, this orientation maximizes the $\pi-\pi$ interaction with graphite, while the reason for the small angular displacement is again due to the steric encumbrance of the methyl groups jutting out of the phthalocyanine plane.

After examining the conformation of a single complex on graphite, we started to probe the self-assembling behavior studying the evolution of the positions of 24 complexes initially and simultaneously placed on a regular lattice, spaced by 25 Å on the x side and 30 or 35 Å on the y side, on the $72 \times 35 \times 2$ graphite slab, and energy minimized (Figure 5a). As we can see from the

dx.doi.org/10.1021/ja109296c |J. Am. Chem. Soc. 2011, 133, 6603–6612

snapshots in Figure 5b (and movie 2), the SMM immediately started to diffuse on the surface, leading to the formation of several small aggregates, which were still mobile and finally coalesced in a single nanocrystal after about 10 ns. The same dynamic behavior and the shape of the final aggregate were also verified in other simulations with different random initial velocities and restraints on the HOPG atoms movement (see also Section 4 and Figure S3 in Supporting Information), hence we are confident of its reproducibility.

Despite the sample being relatively large for the MD standards (40392 atoms), our aggregate is constituted of only 24 complexes, and its dimensions are then very small in comparison with the real aggregates shown in Figure 2. Its limited size and the presence of several defects (cf. Figure 5A) prevent the exact calculation of crystalline cell and lattice parameters. However, the comparison with the experimental results is rewarding and can indeed be attempted. Besides the spontaneous aggregation process, it is interesting to note that the tendency to grow along directions parallel to the graphite axes is confirmed by the shape of the simulated nanocrystal. The three graphite axes form an angle of 120° among each other, and this is matched in the aggregate through the onset of an apparently hexagonal lattice (scheme in Figure 4). Phthalocyanines are known to form either hexagonal or rectangular lattices or both;[38] in this case we cannot distinguish between the two but only estimate the distances between the first and the second neighbors in the crystal (A = 19.5 ± 1 and B = 33 ± 2 Å). These values, assigned by inspecting the radial distribution of Tb atoms (Figure S2 in Supporting Information), are compatible within the error bars with both rectangular and hexagonal lattices, both possibilities being in good agreement with the morphology experimentally observed by STM. Interestingly, the lattice size is slightly shorter than the length of the Pc arm (estimated to be 22.8 Å), and this is accomplished through the in-plane interdigitation of the acetal groups, for a presumed total area per molecule of 342 ± 30 Å^2. Again, the lattice size is in good agreement with the row to row distance measured by STM (see Figure 3). Concerning the height of the aggregate, the calculated topography map in Figure 5B is again in agreement with the experimental results of Figure 1, showing maximum heights of the order of 10 Å (1 nm) in correspondence of the acetal methyl groups. In a last series of calculations we investigated the origin of the growth of the crystals along the graphite axis. To this end we estimated the energy landscape for positioning a new complex close to an aggregate of eight molecules aligned with a graphite axis; the obtained energy map (Figure S2 in Supporting Information) indicates that there are no preferable growth directions from an energetic point of view, i.e., the energy gain for adding a ^{i}Pc$_2$Tb to a formed 2D crystal (approximately 10 kcal/mol) does not depend on the orientation and the position of the complex with respect to the nanocrystal axes. To evaluate also the kinetic effects, we ran a simulation of a single complex on graphite at 500 K and studied its diffusion on the surface as function of the orientation with respect to the graphite axes. It turned out that diffusion is indeed faster along these three directions; these results let us suppose that the shape of the 2D crystals is not due to energetically favorable directions of growth but templated by graphite through an interplay of energetic (the propensity of the complex to move over the graphite surface in a given set of preferred directions largely reflects the binding energy of the complex to the surface) and kinetic effects (the resulting faster diffusion along graphite axes).

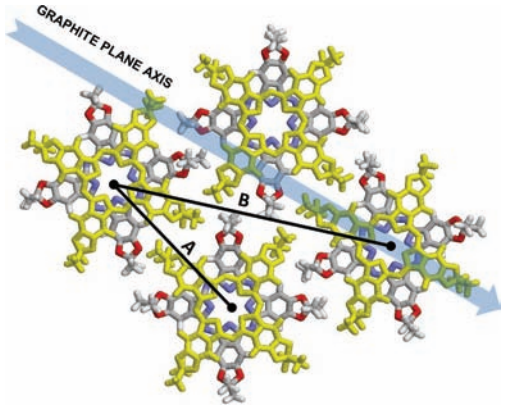

Figure 4. Scheme of the 2D aggregation of ^{i}Pc$_2$Tb complexes on HOPG obtained from MD simulations (the terbium ions are not shown). The ^{i}Pc^{2-} lying directly on graphite (depicted in yellow) has one arm on average parallel to the graphite axis, and this direction corresponds to the favorite direction of growth of the aggregate. The uppermost ^{i}Pc^{2-} (colored following the Corey–Pauling–Koltun scheme) is twisted by about 45° with respect to the growth direction. These 2D crystals present an approximately hexagonal lattice with side A = 19.5 ± 1 Å (B = 33 ± 2 Å).

Magnetic Behavior. The well-defined morphology of the submonolayers of complex ^{i}Pc$_2$Tb is a good example of a low-dimensional assembly of independent SMMs. For this reason, the magnetic behavior of these 2D crystals is very interesting

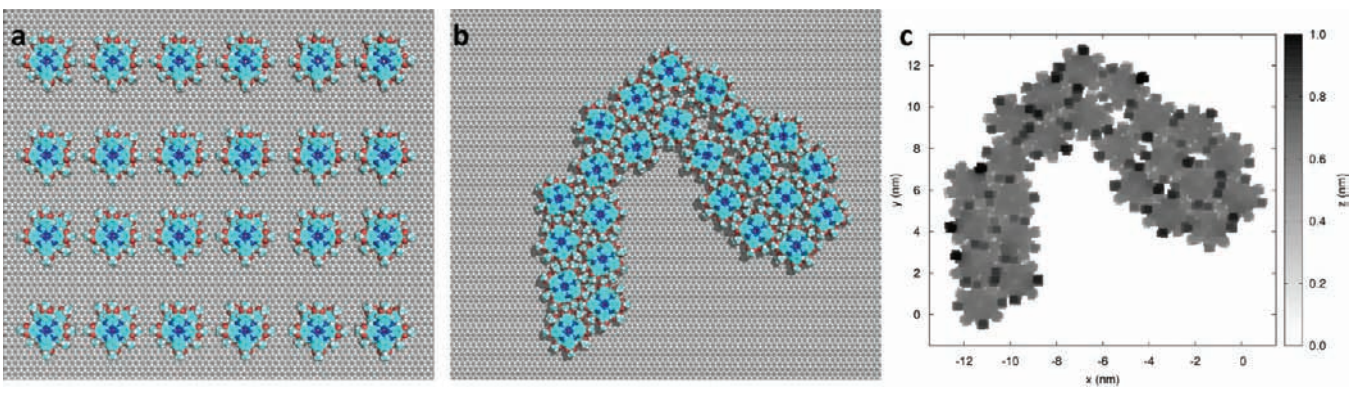

Figure 5. (a) Initial placement of complexes before the MD aggregation simulation. (b) 2D nanocrystals formed by 24 molecules after 10 ns. (c) Calculated topography map of (b), showing that the maximum height of the 2D aggregate is about 1 nm.

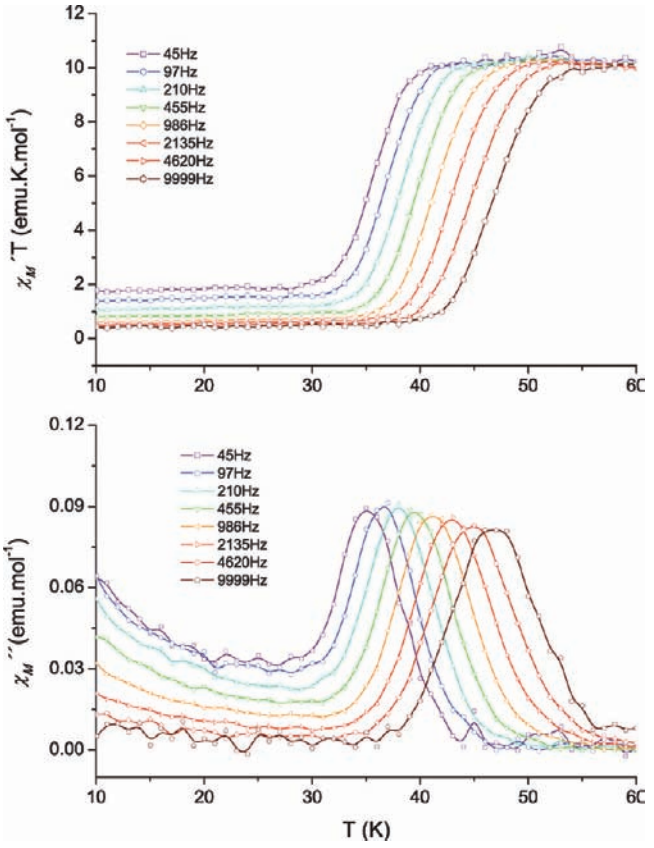

Figure 6. Temperature and frequency dependence of the in-phase (above) and out of phase (below) ac magnetic susceptibility of a microcrystalline bulk sample of **1**.

from the magnetic point of view. It is worth mentioning that all molecules of complex $^{i}Pc_2Tb$ lay directly on the graphite surface, and therefore all of them could be affected by it in some way. It is of great importance to know whether they retain their SMM behavior under such conditions.

Before doing such a study, we characterized the dynamic magnetic behavior of a bulk sample of complex $^{i}Pc_2Tb$ by ac-magnetic susceptometry (see Figure 6).

The blocking temperature of complex $^{i}Pc_2Tb$ in the solid state at 986 Hz was found to be 41 K, which is significantly smaller than the literature value (49 K) for the unsubstituted neutral double-decker terbium complex Pc_2Tb **5** at almost the same frequency (997 Hz) and under the same conditions.[39] Indeed it means that the relaxation time of $^{i}Pc_2Tb$ at 49 K is approximately 3.4×10^{-5} s, 30 times smaller than the literature value of 1×10^{-3} s for Pc_2Tb. The Arrhenius analysis (see Figure 7) showed that the magnetic relaxation of compound $^{i}Pc_2Tb$ in a bulk sample follows a thermally activated process with a pre-exponential factor of $\tau_0^{-1} = 2.61 \times 10^{11}$ s^{-1} and an effective barrier height of $\Delta = 556$ cm^{-1}. This process could be fitted by a Debye function with dispersion parameter $\alpha = 0.11$, as a Cole−Cole plot (see Supporting Information).

The values obtained from the Arrhenius analysis are both significantly higher than those found for a powder sample of the unsubstituted neutral Pc_2Tb complex, 6.8×10^{8} s^{-1} and 410 cm^{-1}, respectively, explaining the apparent different relaxation rates exhibited by the two SMMs. The hysteresis of magnetization of a bulk sample of complex $^{i}Pc_2Tb$ was first recorded at 7 K as a control experiment.

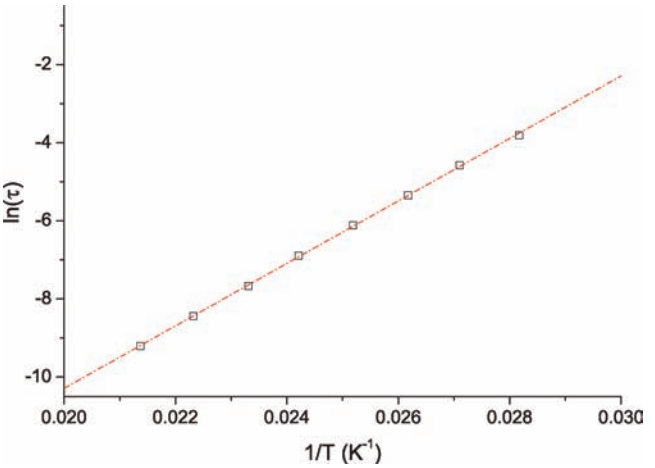

Figure 7. Arrhenius plot of the natural logarithm of the relaxation time τ of complex **1**.

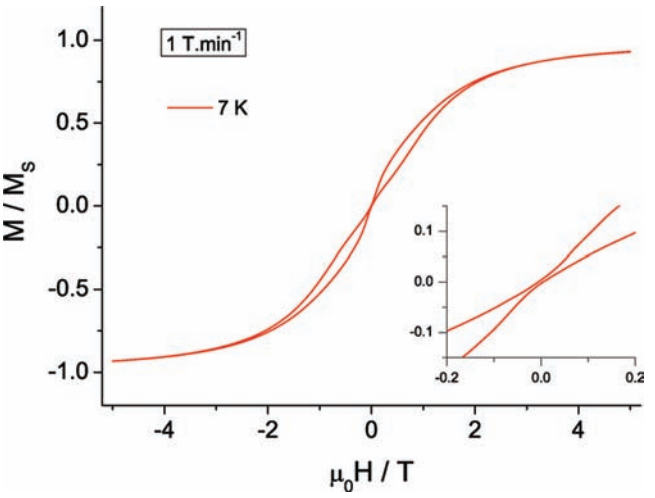

Figure 8. Bulk magnetization hysteresis of a microcrystalline bulk sample of **1** measured at 7 K. Inset: Zooming of the region at low-magnetic fields.

The obtained magnetization hysteresis curve is shown in Figure 8. A butterfly shaped hysteresis,[40] typical in these complexes,[15] was observed. Thus, the magnetization collapses at $\mu_0 H = 0$ T, where almost no coercive field can be observed.

In order to characterize the magnetic response of molecules of complex $^{i}Pc_2Tb$ deposited on a HOPG surface, two samples were prepared: a submonolayer sample, named as ^{ML}**1**, prepared in the dropcasting conditions described earlier, and a thick layer sample ^{TL}**1**, prepared by repeating 10 times the previous dropcasting procedure with a more concentrated (10^{-3} M) solution of **1**.

The differences between samples ^{ML}**1** and ^{TL}**1** should indicate the influence of the surface on the magnetic behavior of the molecules. Indeed, while the submonolayer ^{ML}**1** must be strongly influenced by the interaction of all the molecules of the nanoislands with the surface, the thick layer should behave essentially like the bulk compound in which the majority of molecules only feel the neighboring analogous molecules.

The two samples were studied by XMCD spectroscopy.[41] In this technique, two circularly polarized XAS of complex **1** are measured at the $M_{4,5}$ edge of Tb^{3+} ion with the helicity of the

dx.doi.org/10.1021/ja109296c |J. Am. Chem. Soc. 2011, 133, 6603–6612

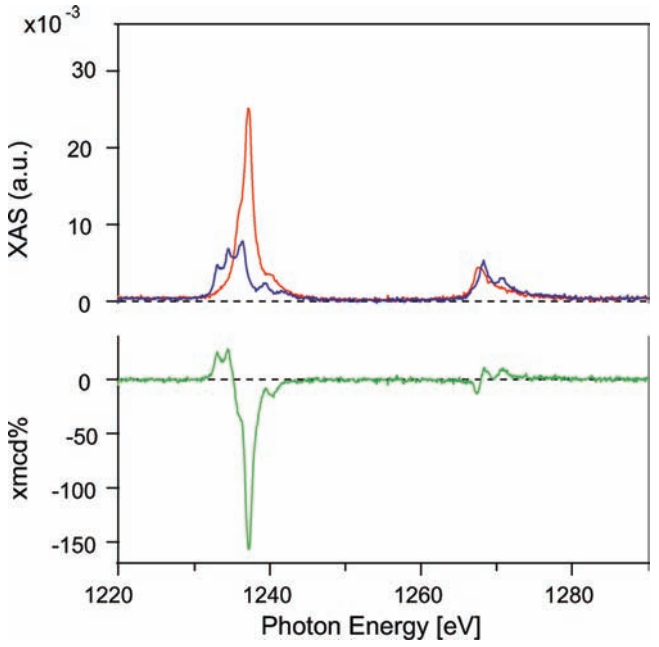

Figure 9. XAS spectra at the $M_{4,5}$ edge of Tb for ^{ML}**1** with helicities parallel ($I^{\uparrow\uparrow}$, in red) and antiparallel ($I^{\uparrow\downarrow}$, in blue) to an applied magnetic field of 5 T at 7 K (above), and the XMCD spectrum given by their difference normalized to the maximum intensity of the unpolarized spectrum $1/2(I^{\uparrow\downarrow} + I^{\uparrow\uparrow})$ (below in green).[42]

incident radiation parallel and antiparallel to the applied magnetic field, respectively. The difference between these two spectra, normalized to the maximum intensity of the unpolarized spectrum, provides the XMCD spectrum (see Figure 9). The incident X-ray photon excites a 3d core electron to the 4f level, and therefore it gives information on the 4f electronic structure governing the magnetic behavior of the terbium ion. The direction of the impinging beam was parallel to the applied magnetic field (H), and both were perpendicular to the sample surface. If the XMCD spectrum holds its shape, then its intensity is proportional to the projection of the magnetic moment of the absorbing atom on the direction of the photon wave vector,[33] and therefore the hysteresis curves can be obtained by recording the XMCD spectrum as a function of the applied magnetic field. The acquisition of the full spectra, however, is time-consuming. A way to speed-up the measurements was the acquisition of the maximum value of the XMCD spectrum by recording the XAS intensity at only two points for each magnetic field value, instead of acquiring the full XAS spectrum, namely at a pre-edge point (1225 eV) and at the energy corresponding to the maximum value of the XMCD signal (1237.6 eV). This is done cycling twice the magnetic field, one cycle for each photon polarization. The intensity values were registered while maintaining the field constant. We adopted this procedure after having checked that the shape of the XMCD spectrum remains the same while varying the magnetic field. A detailed study of the XMCD spectrum of **1** is described elsewhere.[42] In that work, in particular, we proved that the maximum value of the Tb dichroic spectrum is actually proportional to the total Tb magnetization. The hysteresis of XMCD signal was then obtained at an average speed of 1.0 T.min^{-1}.

The obtained XMCD detected magnetization curves, recorded for $|\mu_0 H| \leq 5$T, as described above, are shown in Figure 10.

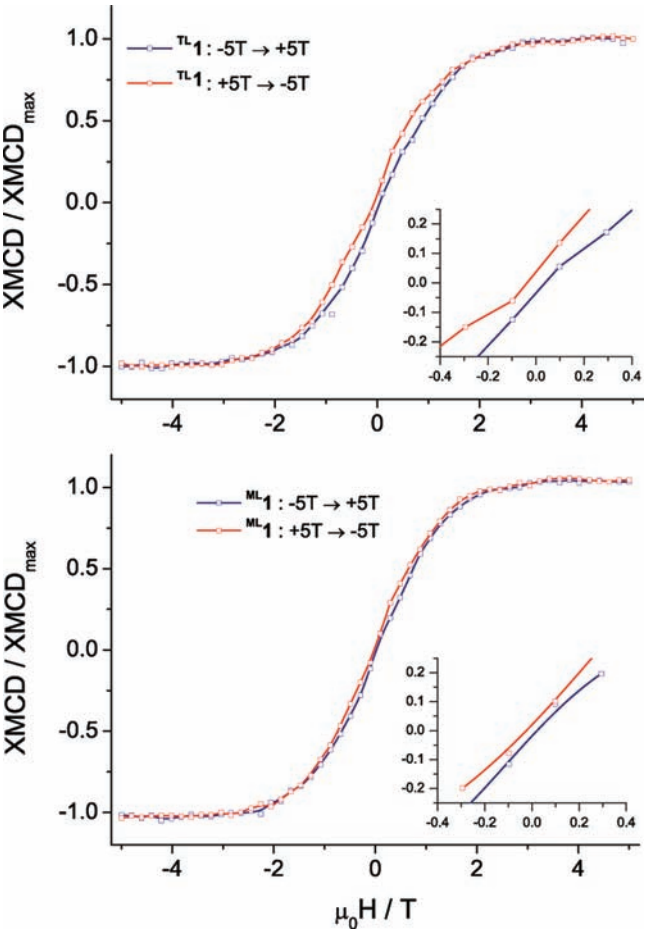

Figure 10. XMCD detected hysteresis of magnetization for the thick layer sample ^{TL}**1** (above) and the monolayer sample ^{ML}**1** (below) on HOPG measured at 7 K (see text). The inset shows the enlargement of the central part of both hystereses.

At first glance, the hysteresis curves of ^{ML}**1** and ^{TL}**1** samples look quite similar in shape. However, it is worth noting that the butterfly loops are more open for the thick film ^{TL}**1** than for the submonolayer sample ^{ML}**1**. There is almost no remnant magnetization for either of the two samples in these conditions, and the coercive field of the submonolayer sample (see inset in Figure 10) is not significantly different from zero, which is to be expected at this temperature (see the 7 K bulk measurement inset in Figure 8).

While they differ slightly from one another, ^{ML}**1** and ^{TL}**1** are both very similar to the bulk measurement made in the same conditions (7 K), which means that the magnetic behavior of **1** is essentially preserved when deposited on the graphite surface. As it appears, there is therefore not much influence of the surface on the magnetic properties of complex **1**, the interaction between the surface and molecules not being able to annihilate the SMM behavior.

■ CONCLUSIONS

The double-decker phthalocyanine lanthanide complex $^{i}Pc_2Tb$ self-assembled on HOPG forms highly regular rectangular 2D nanocrystals that are aligned with the three main graphite axes. XMCD was used as a successful tool to record the magnetization

hysteresis of the complex $^{i}Pc_2Tb$ adsorbed onto the graphite surface.

Unlike the previously described Fe_4 on gold,[43] it is important to notice that here the terbium complexes are not wired covalently to the surface by a long alkyl chain but are on the contrary lying directly on top of the graphite surface. In principle, the perturbation induced by the surface on $^{i}Pc_2Tb$ could have destroyed the SMM properties, but the XMCD magnetization hysteresis measurements showed that this is not the case and, therefore, that this assembly procedure is an interesting one for the preparation of SMM arrays.

Two very recent contributions present the magnetic behavior of nonsubstituted double-decker complexes on Au(111) and Cu(100),[9,13] showing that $TbPc_2$ does not present any hysteresis of magnetization when deposited on Cu(100), while on Au(111) it is clearly observed. It is worth noting the presence of an open butterfly hysteresis both in thick and thin layers of $TbPc_2$ on Au(111). The latter shows a narrower hysteresis than the former one; a result which is consistent with those presented here.

To the best of our knowledge, it is the first time that magnetization hysteresis is observed for molecules of a double-decker phthalocyanine lanthanide complex that are all in intimate contact with a graphite surface. Importantly, the slow magnetic relaxation rate, characteristic of these compounds is still present in a well-characterized submonolayer sample of the neutral $^{i}Pc_2Tb$ complex, and the behavior of the sample is not very different from the bulk complex measured in the same conditions.

■ ASSOCIATED CONTENT

Ⓢ Supporting Information. Complete reference no. 26; Calculation of the potential for torsions involving aromatic nitrogens in phthalocyaninates; In plane radial distribution of aggregates; Potential energy map for adding a new complex to an aggregate of 8 $^{i}Pc_2Tb$; Measurement of the diffusion of a single complex on graphite; and Cole−Cole plot at 40 K for a microcrystalline sample of $^{i}Pc_2Tb$. This material is available free of charge via the Internet at http://pubs.acs.org.

Ⓦ Web Enhanced Feature. Movies of the MD self-assembling and aggregation experiments are available in the HTML version of this article.

■ AUTHOR INFORMATION

Corresponding Author

amabilino@icmab.es (D.B.A.); vecianaj@icmab.es (J.V.)

Present Addresses

[#]School of Chemistry, University of Nottingham, University Park, NG7 2RD Nottingham, United Kingdom.

■ ACKNOWLEDGMENT

This work has been carried out within the 6th and 7th FPs of the EU, under contracts MAGMANet (no. 515767), FuMaSSEC (MEST-CT-2005-020992), EU Large Project ONE-P (FP7-NMP-2007-212311) and also supported by Spanish projects EMOCIONA (CTQ2006-06333/BQU), POMAs (CTQ22010-19501), the Generalitat de Catalunya AGAUR (2009SGR-00516), and the CIBER de Bioingeniera, Biomateriales y Nanomedicina (CIBER-BBN), promoted by ISCIII, Spain. D.S, L.M., and C.Z. acknowledge Stefano Zacchini (University of Bologna) for useful suggestions. We warmly thank Amable Bernabé (ICMAB-CSIC) for recording IR and LDI-TOF spectra. We acknowledge the ESRF for the provision of beamtime, and we are grateful to J.C. Cezar (ESRF) for his precious assistance in using beamline ID8.

■ REFERENCES

(1) Gatteschi, D.; Sessoli, R.; Villain, J. *Molecular Nanomagnets*; Oxford University Press: Oxford, U.K., 2006.
(2) Gatteschi, D.; Bogani, L.; Cornia, A.; Mannini, M.; Sorace, L.; Sessoli, R. *Solid State Sci.* **2008**, *10*, 1701.
(3) Gatteschi, D.; Sessoli, R. *Angew. Chem., Int. Ed.* **2003**, *42*, 268.
(4) Cavallini, M.; Gomez-Segura, J.; Ruiz-Molina, D.; Massi, M.; Albonetti, C.; Rovira, C.; Veciana, J.; Biscarini, F. *Angew. Chem., Int. Ed.* **2005**, *44*, 888.
(5) Affronte, M. *J. Mater. Chem.* **2009**, *19*, 1731.
(6) Rocha, A. R.; Garcia-Suárez, V. M.; Bailey, S. W.; Lambert, C. J.; Ferrer, J.; Sanvito, S. *Nat. Mater.* **2005**, *4*, 335.
(7) Bogani, L.; Wernsdorfer, W. *Nat. Mater.* **2008**, *7*, 179.
(8) Gatteschi, D.; Cornia, A.; Mannini, M.; Sessoli, R. *Inorg. Chem.* **2009**, *48*, 3408.
(9) Margheriti, L.; Chiappe, D.; Mannini, M.; Car, P.; Sainctavit, P.; Arrio, M. A.; de Mongeot, F. B.; Cezar, J. C.; Piras, F. M.; Magnani, A.; Otero, E.; Caneschi, A.; Sessoli, R. *Adv. Mater.* **2010**, *22*, 5488.
(10) Katoh, K.; Komeda, T.; Yamashita, M. *Dalton Trans.* **2010**, *39*, 4708.
(11) Mannini, M.; Pineider, F.; Sainctavit, P.; Danieli, C.; Otero, E.; Sciancalepore, C.; Talarico, A. M.; Arrio, M.-A.; Cornia, A.; Gatteschi, D.; Sessoli, R. *Nat. Mater.* **2009**, *8*, 194.
(12) Vitali, L.; Fabris, S.; Conte, A. M.; Brink, S.; Ruben, M.; Baroni, S.; Kern, K. *Nano Lett.* **2008**, *8*, 3364.
(13) Stepanow, S.; Honolka, J.; Gambardella, P.; Vitali, L.; Abdurakhmanova, N.; Tseng, T.-C.; Rauschenbach, S.; Tait, S. L.; Sessi, V.; Klyatskaya, S.; Ruben, M.; Kern, K. *J. Am. Chem. Soc.* **2010**, *132*, 11900.
(14) Ishikawa, N.; Sugita, M.; Ishikawa, T.; Koshihara, S.-Y.; Kaizu, Y. *J. Phys. Chem. B* **2004**, *108*, 11265.
(15) Ishikawa, N.; Sugita, M.; Wernsdorfer, W. *Angew. Chem., Int. Ed.* **2005**, *44*, 2931.
(16) Ishikawa, N. *Polyhedron* **2007**, *26*, 2147.
(17) Gonidec, M.; Davies, E. S.; McMaster, J.; Amabilino, D. B.; Veciana, J. *J. Am. Chem. Soc.* **2010**, *132*, 1756.
(18) Gomez-Segura, J.; Diez-Perez, I.; Ishikawa, N.; Nakano, M.; Veciana, J.; Ruiz-Molina, D. *Chem. Commun.* **2006**, 2866.
(19) Klymchenko, A. S.; Sleven, J.; Binnemans, K.; De Feyter, S. *Langmuir* **2006**, *22*, 723.
(20) Ivanov, A. V.; Svinareva, P. A.; Zhukov, I. V.; Tomilova, L. G.; Zefirov, N. S. *Russ. Chem. Bull. Int. Ed.* **2006**, *55*, 281.
(21) Kowall, T.; Foglia, F.; Helm, L.; Merbach, A. E. *J. Phys. Chem.* **1995**, *99*, 13078.
(22) Gaunt, A. J.; Reilly, S. D.; Enriquez, A. E.; Scott, B. L.; Ibers, J. A.; Sekar, P.; Ingram, K. I. M.; Kaltsoyannis, N.; Neu, M. P. *Inorg. Chem.* **2007**, *47*, 29.
(23) Paschoal, C. W. A.; Diniz, E. M. *J. Phys.: Condens. Matter* **2009**, *21*, 075901.
(24) Wang, J.; Wolf, R. M.; Caldwell, J. W.; Kollman, P. A.; Case, D. A. *J. Comput. Chem.* **2004**, *25*, 1157.
(25) Cramer, C. J. *Essentials of Computational Chemistry: Theories and Models*; John Wiley & Sons Ltd.: Chichester, U.K., 2004.
(26) Frisch, M. J. et al. *Gaussian 09*, revision A.1; Gaussian, Inc.: Wallingford, CT, 2009.
(27) van Veggel, F. C. J. M.; Reinhoudt, D. N. *Chem.−Eur. J.* **1999**, *5*, 90.
(28) Loosli, C.; Liu, S. X.; Neels, A.; Labat, G.; Decurtins, S. *Z. Kristallogr. - New Cryst. Struct.* **2006**, *221*, 135.
(29) Lukesh, J. S.; Pauling, L. *Am. Mineral.* **1950**, *35*, 125.
(30) Steele, W. A. *J. Phys. Chem.* **1978**, *82*, 817.
(31) Palermo, V.; Biscarini, F.; Zannoni, C. *Phys. Rev. E* **1998**, *57*, R2519.

(32) Phillips, J. C.; Braun, R.; Wang, W.; Gumbart, J.; Tajkhorshid, E.; Villa, E.; Chipot, C.; Skeel, R. D.; Kalé, L.; Schulten, K. *J. Comput. Chem.* **2005**, *26*, 1781.
(33) Chen, C. T.; Idzerda, Y. U.; Lin, H.; Meigs, G.; Chaiken, A.; Prinz, G. A.; Ho, G. H. *Phys. Rev. B: Condens. Matter* **1993**, *48*, 642.
(34) Barrett, A. G. M.; Hanson, G. R.; White, A. J. P.; Williams, D. J.; Micallef, A. S. *Tetrahedron* **2007**, *63*, 5244.
(35) Gurek, A. G.; Basova, T.; Luneau, D.; Lebrun, C.; Koltsov, E.; Hassan, A. K.; Ahsen, V. *Inorg. Chem.* **2006**, *45*, 1667.
(36) Sun, D.; Rosokha, S. V.; Kochi, J. K. *J. Phys. Chem. B* **2007**, *111*, 6655.
(37) Rowland, R. S.; Taylor, R. *J. Phys. Chem.* **1996**, *100*, 7384.
(38) Olivier, Y.; Muccioli, L.; Lemaur, V.; Geerts, Y. H.; Zannoni, C.; Cornil, J. *J. Phys. Chem. B* **2009**, *113*, 14102.
(39) Ishikawa, N.; Sugita, M.; Tanaka, N.; Ishikawa, T.; Koshihara, S.-Y.; Kaizu, Y. *Inorg. Chem.* **2004**, *43*, 5498.
(40) Chiorescu, I.; Wernsdorfer, W.; Müller, A.; Bögge, H.; Barbara, B. *Phys. Rev. Lett.* **2000**, *84*, 3454.
(41) Funk, T.; Deb, A.; George, S. J.; Wang, H.; Cramer, S. P. *Coord. Chem. Rev.* **2005**, *249*, 3.
(42) Biagi, R.; Fernandez-Rodriguez, J.; Gonidec, M.; Mirone, A.; Corradini, V.; Moro, F.; De Renzi, V.; del Pennino, U.; Cezar, J. C.; Amabilino, D. B.; Veciana, J. *Phys. Rev. B* **2010**, *82*, 224406.
(43) Mannini, M.; Pineider, F.; Sainctavit, P.; Danieli, C.; Otero, E.; Sciancalepore, C.; Talarico, A. M.; Arrio, M. A.; Cornia, A.; Gatteschi, D.; Sessoli, R. *Nat. Mater.* **2009**, *8*, 194.